Electrochimica Acta 475 (2024) 143650

Contents lists available at ScienceDirect

Electrochimica Acta

journal homepage: www.journals.elsevier.com/electrochimica-acta

Effect of passivation and surface treatment of a laser powder bed fusion biomedical titanium alloy on corrosion resistance and protein adsorption

Saman Nikpour [a], Jeffrey D. Henderson [b], Sina Matin [a], Heng-Yong Nie [b], Jonas Hedberg [b], Vahid Dehnavi [b,c], Yara K. Hosein [d], David W. Holdsworth [e], Mark Biesinger [a,b], Yolanda S. Hedberg [a,b,*]

[a] *Department of Chemistry, The University of Western Ontario, London, Ontario N6A 5B7, Canada*
[b] *Surface Science Western, The University of Western Ontario, London, Ontario N6G 0J3, Canada*
[c] *Department of Chemical and Biochemical Engineering, The University of Western Ontario, London, Ontario N6A 5B9, Canada*
[d] *Additive Design in Surgical Solutions Centre, The University of Western Ontario, London, Ontario N6G 4X8, Canada*
[e] *Department of Medical Biophysics, The University of Western Ontario, London, Ontario N6A 5C1, Canada*

ARTICLE INFO

Keywords:
Corrosion
Metal release
BSA
EIS
Surface analysis

ABSTRACT

The biomedical titanium alloy Ti6Al4V has excellent corrosion resistance and biocompatibility and is, therefore, widely used in orthopedic and orthodontic implants. Biomedical implants are increasingly fabricated by additive manufacturing, such as laser powder bed fusion (LPBF). These manufacturing protocols often include sandblasting, surface finish, and passivation. This study aims to investigate the effect of different surface finishes and the commonly used ASTM F86–13 nitric acid passivation for LPBF Ti6Al4V on its corrosion resistance, metal release, and surface changes in benign (bovine serum albumin in a pH 7.4 buffer) and harsh (hydrochloric acid at pH 1.5) solutions using various electrochemical and spectroscopic techniques. Electrochemical, solution and surface analysis showed an insignificant effect of passivation. Smooth surfaces exhibited a slightly better corrosion resistance than rough surfaces due to a 10–20 % smaller true surface area and lower protein adsorption. Implanted ceramic beads from the sandblasting procedure remained on the surface even after the mirror-polishing and passivation procedures.

1. Introduction

Strong corrosion resistance, suitable mechanical properties, and biocompatibility are paramount features of titanium and its alloys [1–3]. Commercially pure titanium (CP-Ti) and Ti6Al4V (6 wt. % Al and 4 wt. % V), are suitable for dental implants and total joint replacements, including hip and knee. Due to their relatively low wear resistance, they are typically not employed for articulating surfaces subject to wear [4].

Nonetheless, the biocompatibility of titanium implants is not fully guaranteed since released metallic ions or particles could result in undesirable consequences such as inflammatory reactions, hypersensitivity, and adverse health tissue reactions under physiological circumstances [5–7]. Released metals in the form of either particles, metal ions, or metal complexes with organic species could induce various side effects from local toxicity (metallosis) to systemic toxicity [8]. Those and other clinical effects were reported to be associated with released Ti [9], Al [10], and V [11].

Chemical surface treatments (such as immersion in acidic solutions) are employed to improve the corrosion properties of Ti alloys. The natural thickness of spontaneously formed oxide can be increased, and defect densities decreased, through immersion in different acidic solutions, providing improved biocompatibility [12–14]. This procedure is called passivation since it reduces active corrosion and increases the alloy's passivity, the state of negligible corrosion due to a protective surface oxide. Nitric acid is one of the conventional and standardized passivation procedures that has been widely used in implant industries based on ASTM F86–13. It was previously reported that passivation with nitric acid improved the tribocorrosion behavior of Ti6Al4V [15]. However, Ti6Al4V also naturally passivates in physiological environments and air [16], and it is hence unclear whether passivation is a necessary treatment for biomedical AM Ti6Al4V parts from a corrosion perspective.

---

* Corresponding author at: Department of Chemistry, The University of Western Ontario, London, Ontario N6A 5B7, Canada.
E-mail address: yhedberg@uwo.ca (Y.S. Hedberg).

https://doi.org/10.1016/j.electacta.2023.143650
Received 7 September 2023; Received in revised form 5 December 2023; Accepted 6 December 2023

Moreover, the fabrication process of implants can influence both the mechanical and corrosion performance. Biomedical implants are increasingly fabricated by additive manufacturing (AM) processes [3]. For instance, the laser powder bed fusion (LPBF) technique is utilized to construct intricate and complex structures with utmost precision that can even resemble bone structures [17]. This strategy has facilitated the fabrication of patient-customized implants [18] and maximized the mechanical properties of implants in an unprecedented way [19]. In both conventional and AM approaches, there is an attempt to increase bone osteointegration by altering surface roughness [20,21].

The corrosion of metallic implant materials in a biological environment is impacted by a wide range of physiological processes, such as implant-protein interactions [22], inflammatory reactions [23], and biofilm formation [24]. Proteins may interact with metal ions and metal oxides in different ways throughout the implant's service life, for example with the surface oxide that governs the corrosion properties of implants [25]. Albumin, which is one of the most prevalent proteins found in extracellular tissue fluid, influences the electrochemical behavior of metallic implant materials [26–28].

The design of implants may trigger crevice and pitting corrosion inside confined locations. Modular tapered junctions are known locations for facilitated localized corrosion as they provide restricted areas for electrolyte access [29]. Accumulation of protons inside crevices due to hydrolysis of metal cations generates an acidic condition which attracts negatively charged chlorides and finally disrupts surface oxide stability [16].

This study aims to understand whether surface passivation on smooth and rough surface conditions after LPBF of Ti-6Al-V has any effect on corrosion and metal release under benign physiological conditions in the presence of bovine serum albumin and under harsh conditions simulating crevice circumstances in the presence of HCl.

2. Materials and methods

2.1. *Ti sample preparation*

Inert gas-atomized powder (chemical composition in Table 1) from Renishaw, UK, with a mean particle size of approximately 15–45 μm was used to manufacture square specimens (1.5 × 1.5 × 0.1 cm) of titanium - 6 wt. % aluminum – 4 wt. % vanadium (Ti6Al4V) by Renishaw AM400 Selective Laser Melting System (ADEISS, London, Canada). Post-heat treatment after fabrication was conducted through 5 steps as follows: 1) 60 min gradual heating to 450 °C, 2) 45 min keeping at 450 °C, 3) 45 min reheating to 750 °C, 4) 60 min keeping at 750 °C, and finally 5) cooling down to room temperature inside the furnace. After heat treatment, the sample surfaces were sandblasted by ceramic beads (containing 63–125 μm zirconia, silica at 28–33 wt % and less than 10 wt % alumina).

Half of these specimens received a mirror-smooth surface finish (denoted 'smooth'), and the rest were grit blasted through sandblasting (denoted 'rough', close to natural AM) for preferential bone ingrowth. For each of these groups, half of them were passivated by a 30 min immersion in 30 % nitric acid at room temperature, according to recommendations of ASTM F86–13. Then, samples were cleaned through 5 min sonication in acetone, 5 min sonication in ethanol followed by nitrogen gas drying. The specimens were then investigated with their as-received surfaces. Acronyms of R, RP, S, and SP were used for rough, rough passivated, smooth, and smooth passivated, respectively.

2.2. *Solutions and immersion tests*

For the immersion (metal release) tests, any non-finished surface was sealed with a metal-free, clear nail polish (acrylate), and the solution-exposed surface area was measured (1 cm^2). Exposures were conducted in 5 g/L NaCl (Fisher), 5 mM 2-(*N*-morpholino) ethanesulfonic acid (MES, Sigma Aldrich) buffer at pH 7.4, and 10 g/L bovine serum albumin (BSA, Sigma Aldrich) for 24 h, one week, and four weeks at 25 °C. The specimens were placed in the incubator with gentle bilinear shaking (12°, 22 cycles/min) in darkness to investigate the slower protein-surface interactions. Also, diluted hydrochloric acid (0.027 M HCl 37 %, pH 1.5) was made from HCl 37 %, Sigma Aldrich. Then, specimens were immersed in the HCl solution and placed in the incubator (same conditions as the BSA solution) for 24 h at 25 °C.

Analysis of metal release in solution was conducted in triplicate with a corresponding background control (blank) for each condition, providing three metal specimens and four solution samples for each time point and surface condition. After exposure, the specimens were separated from the solution, rinsed with 1 mL ultrapure water, which was added to the solution to be analyzed to account for metal-rich protein precipitates, dried, and stored in a desiccator before surface analysis. The solution was then frozen (in the case of BSA-containing solution) prior to solution digestion and solution analysis. The HCl solution did not require digestion or acidification.

2.3. *Electrochemical measurements*

The corrosion behavior of different surface conditions was tested in the BSA-containing solution. The Ti6Al4V specimens, a platinum wire, and an Ag/AgCl (saturated KCl) were placed in an electrochemical flat cell as working, counter, and reference electrode, respectively, and connected to Solartron Analytical ModuLab potentiostat. The flat cells were chosen to avoid additional surface preparation and ensure that the surface state was in its as-received form. Open-circuit potential (OCP) measurements versus time were performed for the first 30 min of immersion. After 24 h exposure to the solution, electrochemical impedance spectroscopy (EIS) and potentiodynamic polarization (PDP) were carried out to investigate the integrity of the surface film and protein adsorption. EIS measurements were conducted at OCP and in the 10 kHz–10 mHz frequency range by applying a sinusoidal wave with 10 mV_{rms} amplitude. PDP tests were conducted from −250 to 1500 mV vs. open circuit potential at 1 mV/s scan rate. All measurements were performed at 25 °C. Zview version 3.5 h software was used to fit the EIS data.

2.4. *Surface characterization*

2.4.1. *Laser scanning confocal microscopy*

The surface morphology was measured to estimate the roughness of samples. A laser scanning confocal microscope (ZEISS LSM 800, Carl Zeiss Microscopy GmbH) was employed. The microscope recorded the intensities of a reflected laser beam over a rastered area (983 μm × 983 μm) at 512 × 512 pixels over each optical sectioning of 2 μm in a total sample height range of 180 μm. A 5x lens was used, and the pinhole size was 34 μm. The laser intensity data was converted to surface morphology by finding the height over the optical sectioning, at each pixel over the rastered area, that had the maximum laser intensity. This was done using the instrument-associated software Mountains ConfoMap (version 7.4.8341), and the roughness was calculated according

Table 1
Chemical composition of Ti6Al4V alloy powder provided by the supplier. Bal. – balance.

Element	Al	V	Fe	O	C	N	H	Y	Ti
wt. %	6.33	3.90	0.21	0.11	0.01	0.01	0.002	0.0201	Bal.

to the ISO 25,178–2:2012 standard.

2.4.2. *Scanning electron microscopy (SEM)*

Hitachi SU3900 large chamber variable pressure scanning electron microscopy (SEM) combined with an Oxford ULTIM MAX 65 SDD X-ray analyzer was used for surface and elemental distribution analysis of specimens after electrochemical measurements. A 15 kV electron accelerating voltage and 10 mm working distance were used.

2.4.3. *X-ray photoelectron spectroscopy (XPS)*

XPS was employed to investigate the composition within the 7–10 nm of the surface and protein adsorption characteristics (atomic ratio of nitrogen to specific carbon peaks). Analyses were conducted on two spots for each unexposed coupon and for the coupons exposed for 4 weeks to the protein solution, and for one spot for the coupons exposed to the protein solution for 24 h and 1 week. A Kratos AXIS Supra spectrometer was used to perform XPS analysis. Monochromatic Al K_α X-ray source functioning at 12 mA and 15 kV (180 W) was employed to collect all spectra and pressure was maintained at $\leq 10^{-8}$ Torr during analyses. Photoelectrons, in all spectra, were collected from a 700 × 300 µm area with a 90° take-off angle. Survey spectra were collected using a 1 eV step size and a 160 eV pass energy. High-resolution spectra were collected using a 0.1 eV step size and a 20 eV pass energy. The instrument work function was calibrated to give a binding energy (BE) of 83.96 eV for the Au $4f_{7/2}$ line for metallic gold, and the spectrometer dispersion was adjusted to give a BE of 932.62 eV for the Cu $2p_{3/2}$ line of metallic copper. Charge correction was done against the aliphatic adventitious carbon (C—C) at 284.80 eV. Signal processing and deconvolution were performed by CasaXPS software (version 2.3.24) utilizing a Shirley background. High-resolution spectra of the C 1 s, O 1 s, N 1 s, Ti 2p, and Al 2p were obtained and fitted according to previous papers [30–32].

2.4.4. *X-ray diffraction (XRD)*

The X-ray diffraction (XRD) analyses were conducted utilizing a Rigaku SmartLab X-ray diffraction system, employing Cu K_α radiation at 40 kV and 45 mA. The diffraction data were acquired using grazing incidence X-ray diffraction (GIXRD) with an incident angle of 3° over a 2θ range from 25° to 90° with a step width of 0.02° and a scan speed of 2°/min. The International center for Diffraction Data (ICDD) PDF-4 + 2023 inorganic database was used for phase identification.

2.4.5. *Time of flight secondary ion mass spectroscopy (ToF-SIMS)*

ToF-SIMS (TOF-SIMS IV, ION-TOF GmbH, Germany) was used to find protein fingerprints, hinting towards changes in packing and orientation. Secondary ions were generated by bombarding a pulsed 25 keV Bi_3^+ primary ion beam onto the sample surface. An electric field was used to extract secondary ions, which arrived at the detector by flying through a reflectron tube. Then, the mass to charge ratio (*m/z*) was obtained by converting the arrival times of known species like carbon, hydrogen, and hydrocarbon. To compensate for charge buildup on the sample surface, a flood of a low-energy electron beam was utilized. The chamber base pressure was around 3×10^{-7} mbar. Both positive and negative ion mass spectra in the range of *m/z* 0–900 were collected from areas of 500 µm × 500 µm at a pixel density of 128 × 128 or 256 × 256. H^-, CH^- and C_4H^- for negative and H^+, CH_3^+ and $C_3H_5^+$ for positive were initially used to calibrate the ion mass spectra.

2.5. *Metal release analysis*

The solution was analyzed for trace concentrations of titanium and vanadium by means of inductively coupled plasma mass spectrometry (ICP-MS), after microwave digestion. Aluminum could not be analyzed because of high background levels. Prior to digestion in the Milestone ETHOS UP microwave digestor, 3 mL of each solution was pipetted into an individual tube. In addition, a spike solution was prepared by pipetting 20 µL of 100 ppm quality control stock (QCS) containing titanium and vanadium into 3 mL of the solution to ensure the accuracy of ICP-MS measurements. Then, 333 µL of pure nitric acid (≥ 68 %) was pipetted to 3 mL of solutions in the digester tube. Next, tubes were placed in the digester canisters containing 10 mL of ultrapure water, after that, the digester canisters were placed in the microwave digestor. A thermometer was placed in one of the canisters to control the temperature during digestion. Digestion was performed at 170 °C over 10 min for temperature ramping followed by 10 min maintaining at 170 °C and removed once the temperature cooled below 50° C (based on EPA 3015). After digestion, the final volume was adjusted to 10 mL by adding ultrapure water. Digestion was only done for protein-containing solutions. The dilution factor was calculated by the final volume divided by the initial sample volume.

Agilent 7700 and Thermo Fisher iCAP Q ICP-MS instruments were employed to measure the released amounts of titanium and vanadium in solutions after 24 h, one week, and four weeks of immersion. Recovery of quality control samples were within 15 % of the expected value, and matrix spike and matrix spike duplicates were within 30 % of the control limit. The dilution-adjusted limits of detection were 1.8, 0.07, 18.1, and 0.69 µg/L for titanium in digested protein solution, vanadium in digested protein solution, titanium in hydrochloric acid solution, and vanadium in hydrochloric acid solution, respectively, using the Agilent 7700 instrument; 0.17 and 0.003 µg/L for titanium and vanadium in digested protein solution, respectively, using the Thermo Fisher iCAP Q instrument. The amount of released metal was calculated according to Eq. (1). c_{Sample}, c_{Blank}, DF are sample concentration, blank concentration and dilution factor, respectively. The exposure volume for each specimen was 0.00225 L [33].

$$\text{Amount of released metals}\ \left(\mu g / cm^2\right) = \frac{\left(c_{Sample}\left(\frac{\mu g}{L}\right) - c_{Blank}\left(\frac{\mu g}{L}\right)\right) \times DF \times 0.00225\ (L)}{A\ (cm^2)} \tag{1}$$

2.6. *Contact angle measurements*

Contact angles of ultra-pure water (2 µL) were measured on selected samples at 25 °C using a KRUSS Drop Shape Analyzer (DSA30E). The analyzer’s ADVANCE software was used to measure the static water contact angles and the average of three replicates was reported.

2.7. *Statistical analysis*

The data sets of two different conditions were statistically compared by a student’s *t*-test for unpaired data with unequal variance using KaleidaGraph v. 4.0. If *P* values <0.05, the two data sets were considered to be statistically significantly different.

3. Results and discussion

3.1. *Electrochemical measurements*

The OCP value reflects the equilibrium potential, without applied potential, for which the sum of cathodic and anodic currents is zero. It may change because of changes in either the cathodic or anodic reactions. Without a change of the cathodic current, a smoothly increasing OCP with time, reaching a steady state, typically means that the rate of the anodic reactions is decreasing due to passivation (surface oxide buildup and stabilization). A sudden decrease would mean a “breakdown” due to sudden localized corrosion. A smooth decrease can mean the gradual dissolution of the surface oxide, increasing anodic reactions, or a gradual decrease of the cathodic reactions due to the adsorption of ligands (here, proteins). All specimens in the BSA solution showed relatively stable behavior during immersion in the solution, and the observed values were in the same range as previously reported values [28,34]. The trend of the OCP during 30 mins of exposure to the protein-containing solution did not show any significant differences between all four surface conditions, Fig. S1 (supplementary information).

Fig. 1 shows EIS results after 24 h of immersion in the BSA solution. It can be seen from the Nyquist diagram (Fig. 1a) that all surface conditions exhibited semicircular patterns with a large radius, indicative of strongly passive conditions [35,36], and that they are similar among the surface conditions. Both the Bode plots (Fig. 1b) and Nyquist plots (Fig. 1a) indicate excellent passivity and high corrosion resistance.

The Randle circuit [28,37] was used to fit the EIS spectra. Solution resistance, surface oxide resistance, surface oxide effective capacitance, constant phase element, phase constant exponent, and the accuracy of fitting are denoted as R_s, R_p, C_{eff}, CPE, n, and χ^2. Regarding heterogeneous surface properties, CPE was used to consider non-ideal capacitance for equivalent circuits. C_{eff} values were obtained according to the following equation [38].

$$C_{eff} = Q^{1/n} \times (R_p)^{(1-n)/n} \tag{2}$$

Extracted parameters from the fitting of EIS measurements are depicted in Figs. 1, S2, and Table S1. Effective capacitances were significantly ($P<0.05$) lower for smooth than rough samples but there was no significant difference seen after passivation. A similar trend to C_{eff} was seen for CPE. The impact of passivation is only seen for the surface oxide resistance (R_p) but was not statistically significant.

Lower effective capacitance can be used to infer a more protective and compact oxide since it correlates with the surface oxide thickness according to the following equation [39]:

$$C_{eff} = \varepsilon \times \varepsilon_o \times \frac{A}{d} \tag{3}$$

where ε, ε_o, A, and d are the relative dielectric constant, vacuum permittivity, surface area, and thickness, respectively. Greater values of C_{eff} for rough than smooth samples could be attributed to a larger surface area originating from rough morphology.

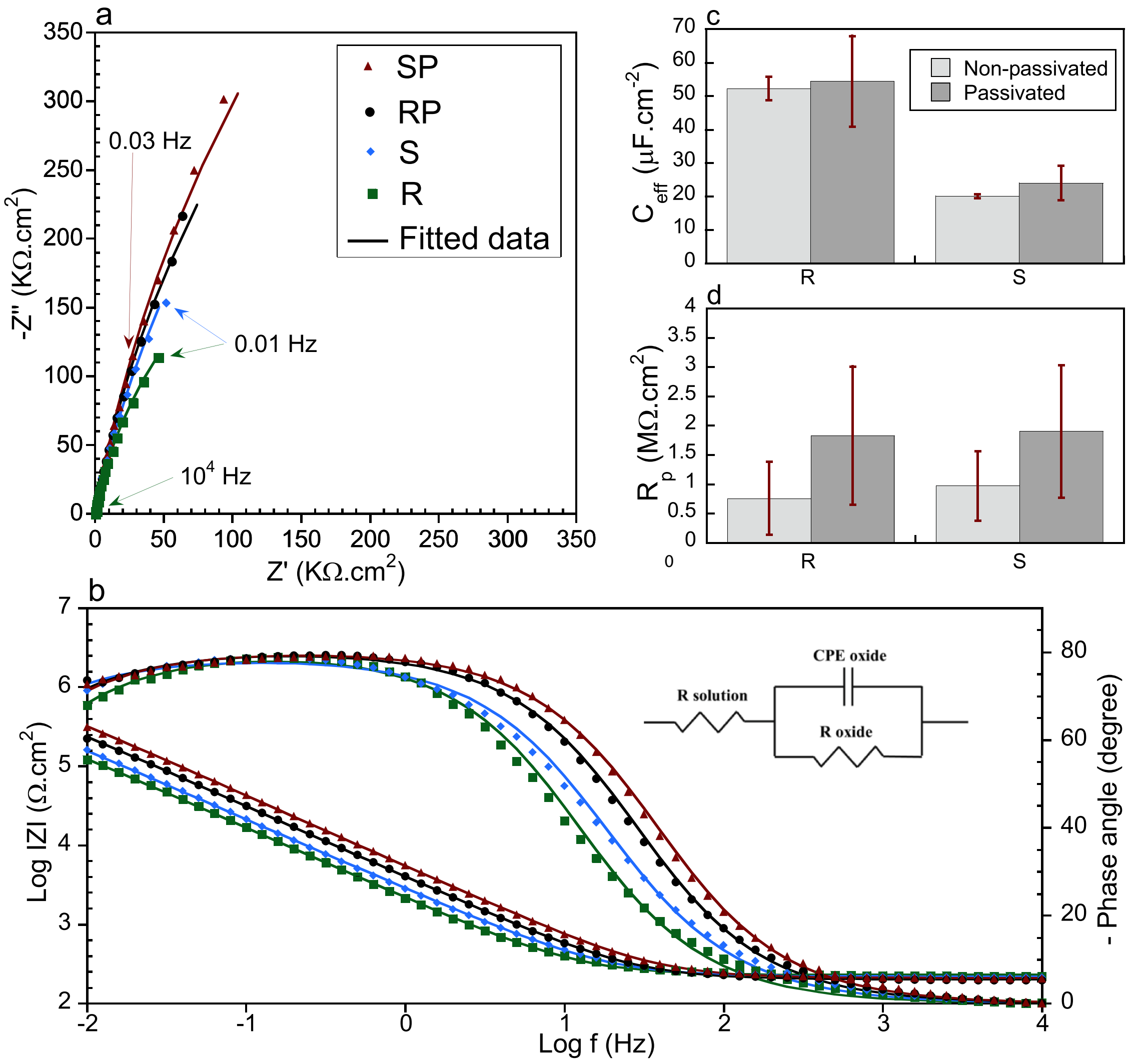

Fig. 1. Representative EIS spectra and extracted parameters after 24 h immersion in protein-containing solution (5 g/L NaCl, 5 mM MES, 10 g/L BSA) for different surface conditions at pH 7.4 and 25 °C. (a) Nyquist diagram (b) Bode plot. Average and standard deviation (error bars) of extracted parameters (effective capacitance and polarization resistance) of three independent specimens (c and d). Corresponding fitting parameter and variability information in Figs. S2 and Table S1.

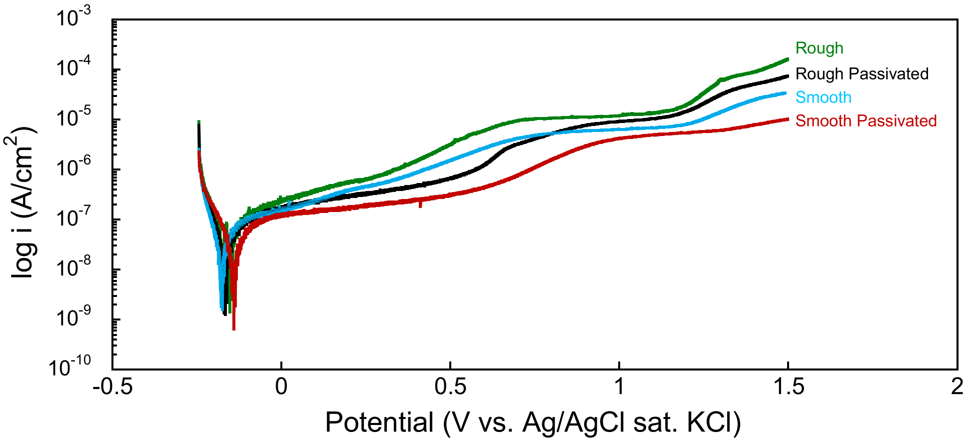

Fig. 2. Representative potentiodynamic spectra of various surfaces after 24 h immersion in the BSA solution (5 g/L NaCl, 5 mM MES, 10 g/L BSA) at pH 7.4 and 25 °C.

Table 2
Calculated corrosion parameters of different surface conditions after 24 h immersion in proteinous solution (5 g/L NaCl, 5 mM MES, 10 g/L BSA) at pH 7.4 and 25 °C, showing mean and standard deviations of three independent specimens and measurements.

Samples	i_{corr} (μA/cm^2)	i_{pass} (μA/cm^2)	E_{corr} (mV)
R	0.02 ± 0.008	0.31 ± 0.11	−173 ± 30
RP	0.02 ± 0.0008	0.24 ± 0.04	−159 ± 40
S	0.01 ± 0.001	0.17 ± 0.06	−138 ± 21
SP	0.01 ± 0.004	0.08 ± 0.007	−210 ± 50

Fig. 2 depicts the potentiodynamic polarization graphs in the neutral BSA solution, showing a strongly passive condition with a long passive region with low passive current density and no breakdown potential for all surfaces in the BSA solution, similar to EIS and literature findings [40, 28].

The corrosion parameters from three independent specimens are listed in Table 2. Smooth specimens exhibited lower corrosion current density than rough samples (statistically significant for passivated surfaces only). The passive current density values (here defined as the value that was 200 mV more positive than the corrosion potential) for passivated specimens were slightly lower than those for non-passivated specimens.

3.2. *Surface characterization*

The XRD spectra for the four samples are depicted in Fig. 3a with the primary peaks corresponding to specific phases labelled. Notably, the observed diffraction peaks exhibit broadening, most likely due to the plastic deformation induced by sandblasting at the sample surfaces. This broadening is attributed to the limited penetration depth of X-rays in GIXRD, focusing on the uppermost surface layers. All examined samples exhibited the presence of the α-phase (ICDD 01–083–4054), characterized by a hexagonal close-packed (HCP) structure. There is a possibility of minor β-phase occurrence with a cubic structure. The primary peak for the β-phase, $(110)_\beta$, is approximately situated at 38.76° (ICDD 01–089–4913), but its identification may be obscured by the broader $(002)_\alpha$ and $(101)_\alpha$ peaks at 38.42° and 40.27°, respectively. The XRD patterns for the smooth and smooth passivated samples reveal additional peaks consistent with zirconium dioxide (ICDD 01–087–7160) with a monoclinic structure. This observation aligns with the EDS results (Tables S2 and S3), indicating elevated concentrations of Zr and O on the surfaces of the smooth and smooth passivated samples.

SEM analysis was performed after electrochemical measurements to see if there were any specific changes to the surface of the samples, Fig. 3b-e. There were no visible changes after the electrochemical polarization to 1.5 $V_{Ag/AgCl}$ compared to the unexposed regions (Fig. S3). According to Fig. 3, rough (b) and rough passivated (c) samples indicated an uneven morphology, while smooth (d) and smooth passivated (e) surfaces did not have irregularities. Observed particles on all surfaces were related to the ceramic beads used for sandblasting and contained Zr, Si, and Al oxide, as shown in the EDS maps in Fig. S4 and Table S3.

The 3D images of the surface morphology deduced from the laser scanning confocal microscopy measurement in Fig. 4 show the difference between the samples in terms of roughness and surface area. The rough surfaces had approximately a 10–20 % greater surface area than the geometrical area, Table 3, and are significantly rougher than the smooth specimens ($P<0.01$). There was no significant effect of passivation on the surface roughness and area of the samples.

The static contact angles of a 2-μL ultrapure water droplet were measured to 81.8 ± 0.9°, 85.4 ± 0.5°, 78.8 ± 1.5° and 79.93±1.0° for R, RP, S, and SP, respectively (examples in Fig. S5). Although these changes are small, this was statistically significant between rough and rough passivated, as well as between rough passivated and smooth passivated ($P<0.01$ in both cases).

The surface composition of specimens after 24 h immersion in both BSA and HCl solutions was studied by XPS. The results from the quantification of survey spectra are presented in Fig. 5a. The most abundant elements were carbon, oxygen, nitrogen, titanium, aluminum, silicon, and zirconium, with their levels depending on exposure conditions. Notably, the levels of carbon and nitrogen were consistently higher for samples exposed to BSA compared to unexposed and HCl-exposed samples. Their relative fraction further increased with immersion time in BSA solution, Fig. 5b. This is possibly due to the protein adsorption processes known to occur during exposure to BSA [41]. The surface composition of HCl-exposed specimens was relatively similar to unexposed ones, Fig. 5a. This is due to the excellent corrosion resistance of titanium alloys [42,43]. Zirconium, silicon, and aluminum may originate from the sandblasting procedure, and silicon is further discussed below.

Fig. 6 focuses on the main alloy elements only, showing the speciation (metallic or oxidic) of titanium and aluminum (vanadium was below the detection limit), after the various exposure durations and for the different specimens. The oxide thickness increased gradually with time, indicated by the lower fraction of metal peaks with time. Throughout the 4 weeks of exposure, the smooth surfaces consistently have a slightly thicker oxide (as evidenced by a lower metal peak fraction) and a higher aluminum oxide ratio than the rough surfaces. There was no significant effect of the passivation on the surface oxide composition, Fig. 6.

After exposure to BSA solution, the ratio between organic nitrogen

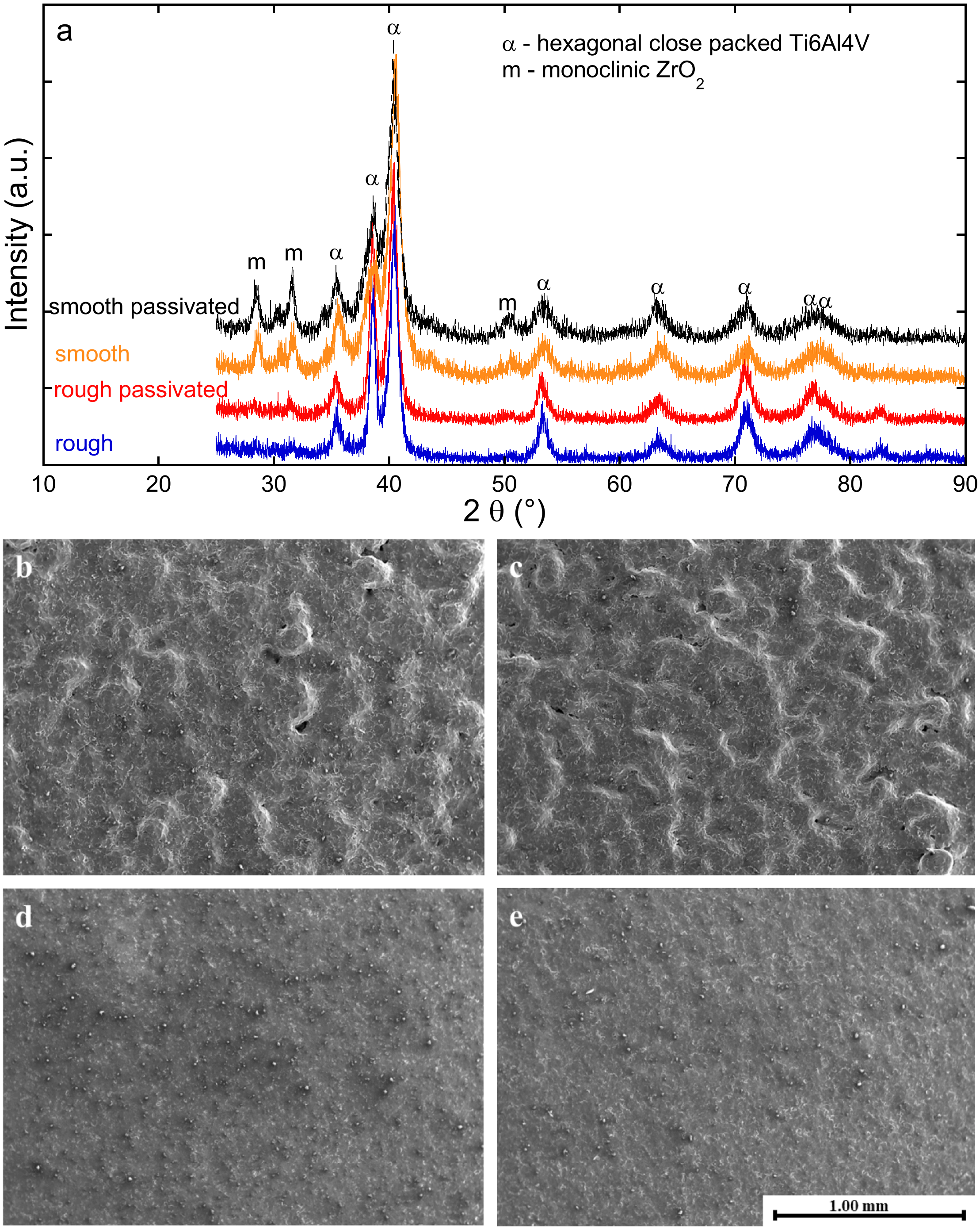

Fig. 3. a) XRD results of unexposed specimens (corresponding SEM and EDS data in Figs. S4 and Table S2). b-e) representative SEM micrographs of different surface preparations; b) rough, c) rough passivated, d) smooth, and e) smooth passivated after 24 h immersion in the BSA solution (5 g/L NaCl, 5 mM MES, 10 g/L BSA) at pH 7.4 and 25 °C.

and higher binding energy carbon (or $N/(C_2+C_3+C_4)$) increased from less than 10 at % to 30–40 at %, indicating BSA adsorption [44], Fig. 7. The theoretical ratio for adsorbed bulk BSA should be 0.48 [45]. This ratio can be defined as the atomic ratio between organic nitrogen to carbon indicating BSA adsorption. Organic N was at 399.86 eV and carbon peaks, C—OH and/or C—O-C, C=O, and O—C=O were at 286.13 eV, 287.89, and 288.75 eV, respectively. However, there is a possible contribution of adventitious carbon, which lowers the measured ratio from the theoretical ratio. The C_1 (C—C and/or C—H at 284.80) was excluded due to the large contribution from adventitious carbon. A typical experimental ratio for a monolayer BSA adsorption was stated to be around 0.4 and approaching higher values, closer to 0.48, with higher solution protein concentration and hence a more fully covered monolayer [46]. Also, BSA adsorption on metals remains as one monolayer due to electrostatic repulsion, hindering the formation of multilayers [47].

After 24 h of immersion, this ratio was similar for all surface conditions, however, after one week and four weeks, it was consistently higher for rough than smooth samples, indicative of more protein adsorption on the rough surfaces.

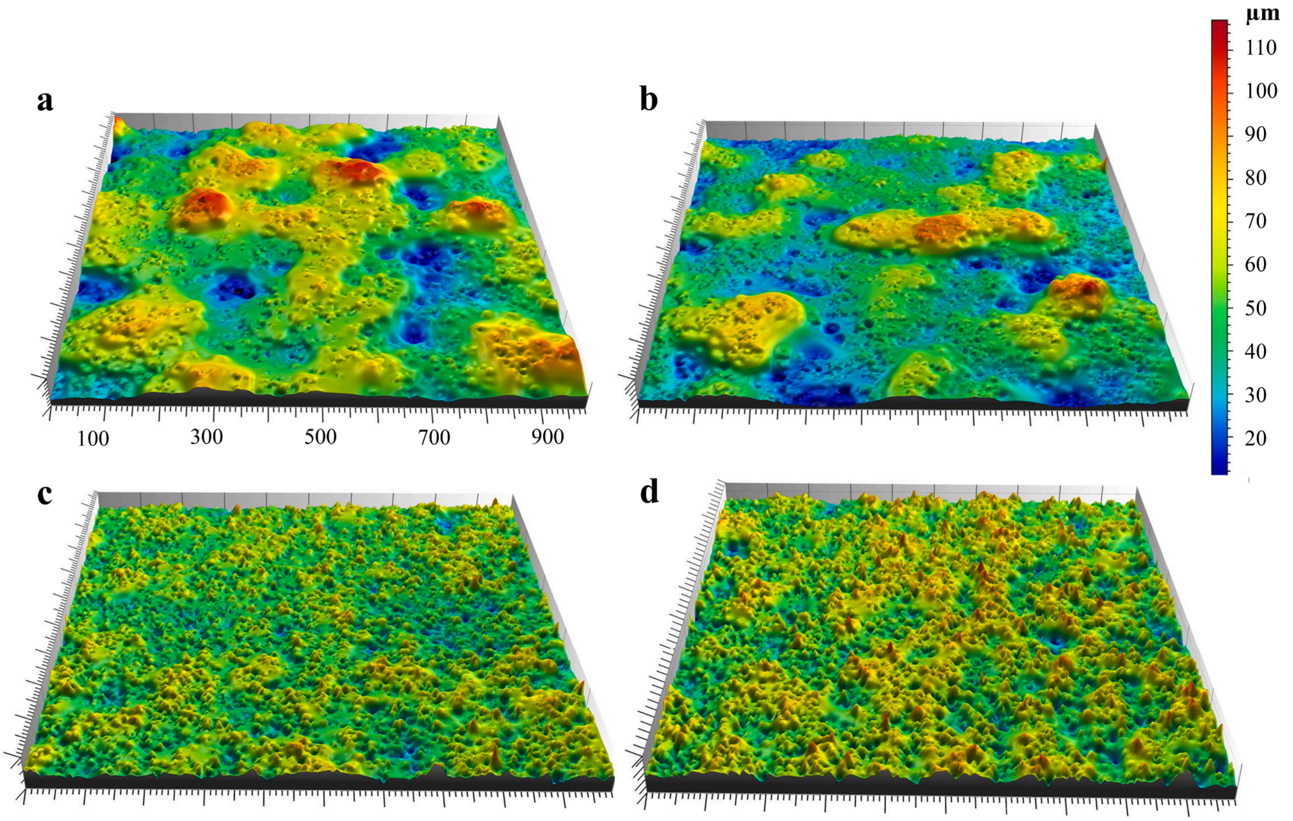

Fig. 4. 3D images of surface morphology of unexposed samples. A) rough, b) rough passivated, c) smooth, and d) smooth passivated.

Table 3
The surface roughness and area of various surface conditions for a 0.010 cm^2 geometrical area. Root mean square roughness and arithmetic roughness are denoted by S_q and S_a. Mean and standard deviation of three independent specimens and measurements.

Samples	S_q (µm)	S_a (µm)	Area (cm^2)
R	23.3 ± 0.6	17.0± 1.0	0.011 ± 0.0009
RP	25.0 ± 0.6	18.0 ± 0.6	0.012 ± 0.001
S	12.3 ± 0.6	8.0 ± 0.2	0.010 ± 0.0005
SP	11.0 ± 0.6	7.0 ± 0.1	0.010 ± 0.0003

For more detailed information about protein adsorption on different surfaces and surface composition, high-resolution spectra of nitrogen, carbon, oxygen, titanium and aluminum at different time slots were compared in Figs. S6–S10. A higher organic nitrogen peak was observed after four weeks (Fig. S6) in rough specimens compared to smooth specimens. Metallic and metal oxide signals for both titanium and aluminum decreased as a function of time which could be related to a thicker or tighter protein layer on the surface [33].

The presence of a peak around 532.4 ± 0.8 eV in the O 1 s spectra was attributed to organic species or silicone [48]. The possible presence of the common silicone contaminant was analyzed by Si 2p high-resolution of one of the surface conditions (Fig. S11). Fig. S11 shows that deconvoluted peaks of Si 2p were placed almost at 102.2–102.9 which probably resulted from silicone [48].

The ToF-SIMS study of the surfaces after exposure to the protein solution revealed that the positive ion mass spectra are more useful than the negative ion counterparts as amino acids fragmented more favorably to positive ions. The ratio of metal oxide to metal, TiO^+/Ti^+, is depicted in Fig. 8a. The intensities of Al^+ detected on all specimens were weak. Exposure to BSA solution increased the TiO^+ signal more for smooth than rough samples ($P<0.05$). A significant effect of passivation was only seen for the smooth surface after 4 weeks of exposure.

The sum of the intensities of positive ions diagnostic to amino acids that represent the protein (Fig. S15) was added and normalized to the total intensity to see the effect of each surface condition on protein adsorption, which is shown in Fig. 8b [49]. Fig. 8b revealed relatively small changes; the only statistically significant changes occurred after one week of immersion, without any clear trend.

3.3. *Metal release*

ICP-MS results for the released amount of metals for different immersion times in BSA solution are depicted in Fig. 9. Passivation reduced the amount of released metal for both titanium and vanadium. The effect of passivation was only statistically significant for the amount of released titanium from the rough condition after one week. In addition, smooth surfaces with or without passivation showed a lower amount of released titanium and vanadium which is consistent with electrochemical and surface analysis.

The released amount of titanium and vanadium was considerably higher in the acidic HCl solution than in the neutral BSA solution, Fig. 10. The difference between BSA and HCl solutions in terms of released amount of titanium and vanadium was statistically significant. Smooth surfaces showed significantly lower released amount of titanium than rough surfaces in HCl solution. Passivation did not change the amount of released metals significantly.

3.4. *Further discussion*

This study showed that rough surfaces had an approximately 10–20 % larger surface area than smooth surfaces. This study further showed more compact protein adsorption on the rough surfaces, by both surface analytical methods (XPS and ToF-SIMS). This is in agreement with other studies [50]. We speculate that protein adsorption could be facilitated because of an increased degree of conformational freedom of adsorbing proteins on rough surfaces with multiple curvatures (less electrostatic

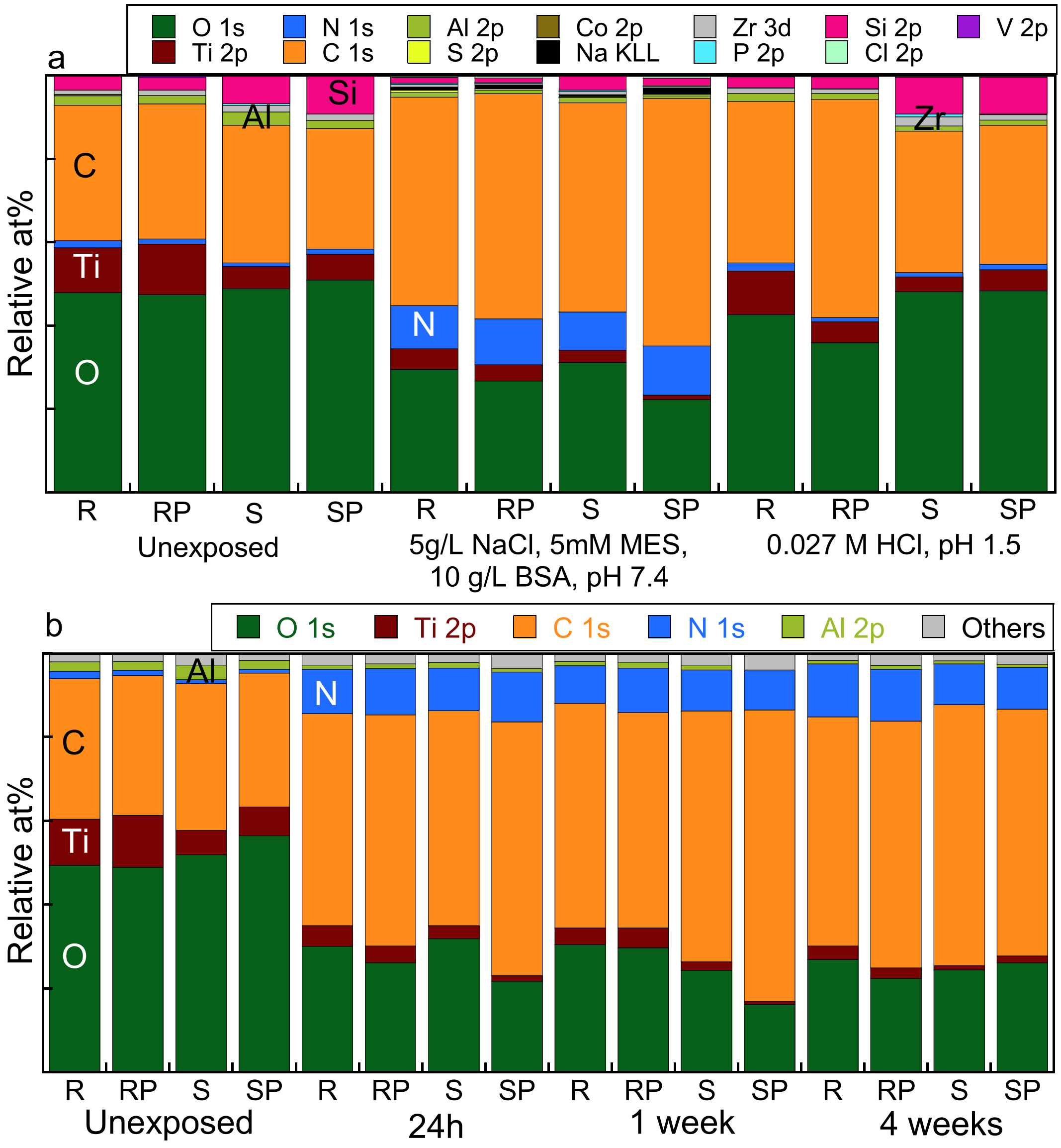

Fig. 5. Comparison of elemental distribution based on XPS wide spectra for the various Ti6Al4V specimens (rough – R; rough passivated – RP; smooth – S; smooth passivated – SP) a) after 24 h immersion in BSA solution (5 g/L NaCl, 5 mM MES, 10 g/L BSA) at pH 7.4 and 0.027 M HCl solution (pH 1.5) at 25 °C, and b) after 24 h, 1 week, and 4 weeks in BSA solution (5 g/L NaCl, 5 mM MES, 10 g/L BSA) at pH 7.4 and 25 °C. The data presented is the average data of two spots (unexposed and 4 weeks) or one spot (24 h and 1 week). For information on variability, see Fig. S12.

repulsion to other protein molecules) [51–53]. Another contributing factor could be the detected surface contamination (silicone and an enrichment of sand blasting ceramic beads) on the smooth surfaces after the mirror-polishing process, possibly hindering protein adsorption.

Our findings further indicated that rough specimens showed slightly inferior behavior from an electrochemical (corrosion resistance) and metal release perspective than smooth surfaces. The true surface area difference alone explains most of the observed differences, which is around 10–20 %. In contrast to other studies in harsher conditions (BSA and hydrogen peroxide) [33,54], this study did not observe any clear effect of protein-induced complexation and surface oxide changes, since the ratio of Al to Ti oxide in the surface oxide remained roughly unchanged. Therefore, it is unlikely that the higher metal release and slightly higher corrosion in rough surfaces are related to the higher protein adsorption on the rough surfaces in this study. Another factor that possibly influenced the slightly higher corrosion susceptibility and metal release of rough surfaces was that the polishing procedure of the smooth surface slightly increased the oxide thickness and aluminum enrichment in the oxide, as evident from both ToF-SIMS and XPS results, hence, acting like a pre-passivation. The stronger adsorption of proteins could further have hindered this natural and additional passivation process in the specimens with the rougher surfaces upon exposure to the protein-containing solution.

Our study showed only a slight impact of passivation on metal release and corrosion behavior, with slightly reduced metal release and barely improved corrosion resistance. It was previously stated that passivation in nitric acid would reduce the surface oxide thickness and increase the released amount of metal ions [55]. However, our study was done on LPBF Ti6Al4V, in a lower concentration nitric acid, and for a shorter time than that study. It has previously been suggested that the combination of various acids could be more effective in terms of corrosion inhibition [14] however, in this study, we saw a very high corrosion resistance and very low metal release for all conditions. Previous studies indicated higher amounts of released metals for wrought Ti6Al4V in the presence of different concentrations of BSA [56]. In addition, higher released amounts of titanium and vanadium were observed for wrought Ti6Al4V in the presence of H_2O_2 and BSA [57]. The metal release in this study after 24 h from LPBF Ti6Al4V in 0.4 %

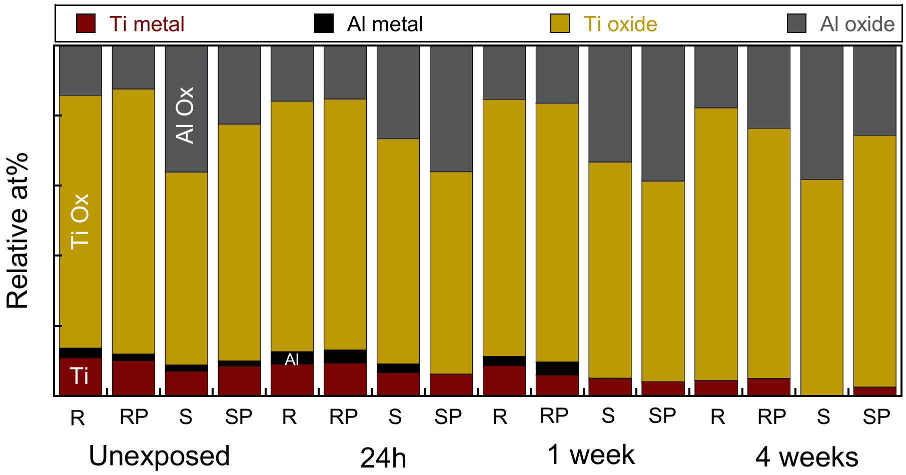

Fig. 6. Surface oxide composition based on XPS high-resolution and wide spectra for each condition after 24 h, 1 week, and 4 weeks in BSA solution (5 g/L NaCl, 5 mM MES, 10 g/L BSA) at pH 7.4 and 25 °C. The data presented is the average data of two spots (unexposed and 4 weeks) or one spot (24 h and 1 week). For information on variability, see Fig. S13.

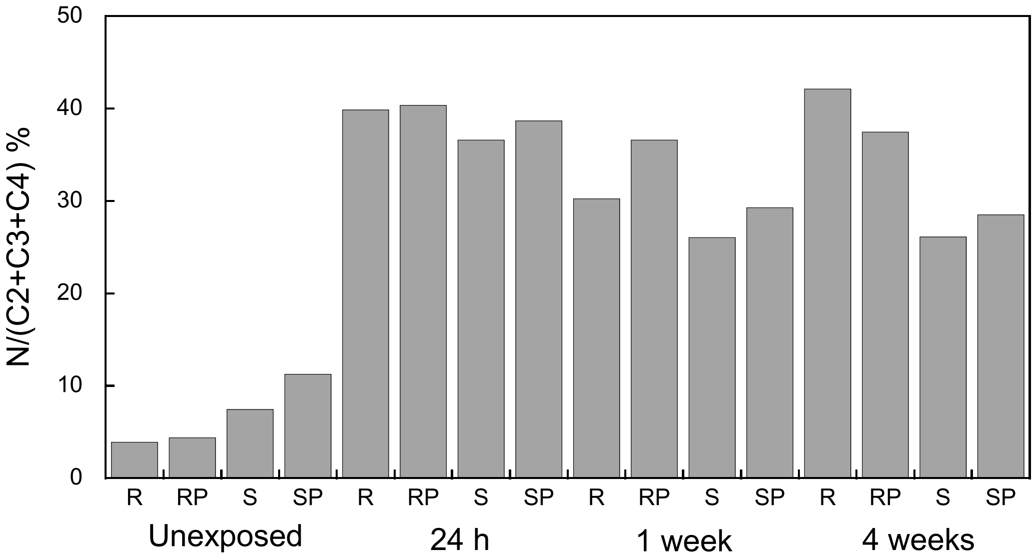

Fig. 7. The atomic ratio between organic nitrogen to carbon for each condition after 24 h, 1 week, and 4 weeks in BSA solution (5 g/L NaCl, 5 mM MES, 10 g/L BSA) at pH 7.4 and 25 °C. The data presented is the average data of two spots (unexposed and 4 weeks) or one spot (24 h and 1 week). For information on variability, see Fig. S14.

HCl was comparable to a study on traditionally manufactured Ti6Al4V in 0.01 % HCl after one week [58]. The specimens in this study were manufactured using a biomedical protocol, including sandblasting. SEM and XPS results suggested that ceramic beads from the sandblasting were found abundantly on all surfaces, including the smooth (polished) ones, the passivated surfaces, and the ones that have been exposed to solution for up to 4 weeks. This is in line with previous studies showing inclusions consisting of silicon, zirconium and aluminum from sandblasting remained on the surface [59,60]. There are several clinical implications of these incorporated ceramic beads. First, they can act as three-body wear (small, hard particles between two surfaces) in a fretting situation, where two surfaces rub against each other. This would worsen corrosion types that involve friction such as tribocorrosion and mechanically assisted crevice corrosion [29,61]. Second, it has been reported that the presence of sandblasting inclusions on rough surfaces could alter the electrochemically active area of the surface and yield higher capacitance [62]. This mechanism would not even require any mechanical action. A previous study suggested that modified nitric passivation could remove all inclusions which was not observed in this study using 30 % nitric acid at 25 ºC for 30 min [60].

While this study, under passive conditions, showed no large effect of passivation and surface preparation, it remains to be investigated how these factors influence corrosion under worse conditions, such as under friction, which should be investigated in future studies.

In addition to sole corrosion effects, passivation also influences the level of adherent endotoxins on titanium implant surfaces and passivation has been reported to be an efficient way to remove these endotoxins [63]. Therefore, this study should not be used as a justification for omitting passivation procedures that might be necessary for biomedical implant surfaces.

4. Conclusions

After evaluating the effect of passivation on LPBF Ti6Al4V with different surface conditions (rough and smooth) in BSA (pH 7.4) and HCl (pH 1.5) solutions, the following conclusions were drawn:

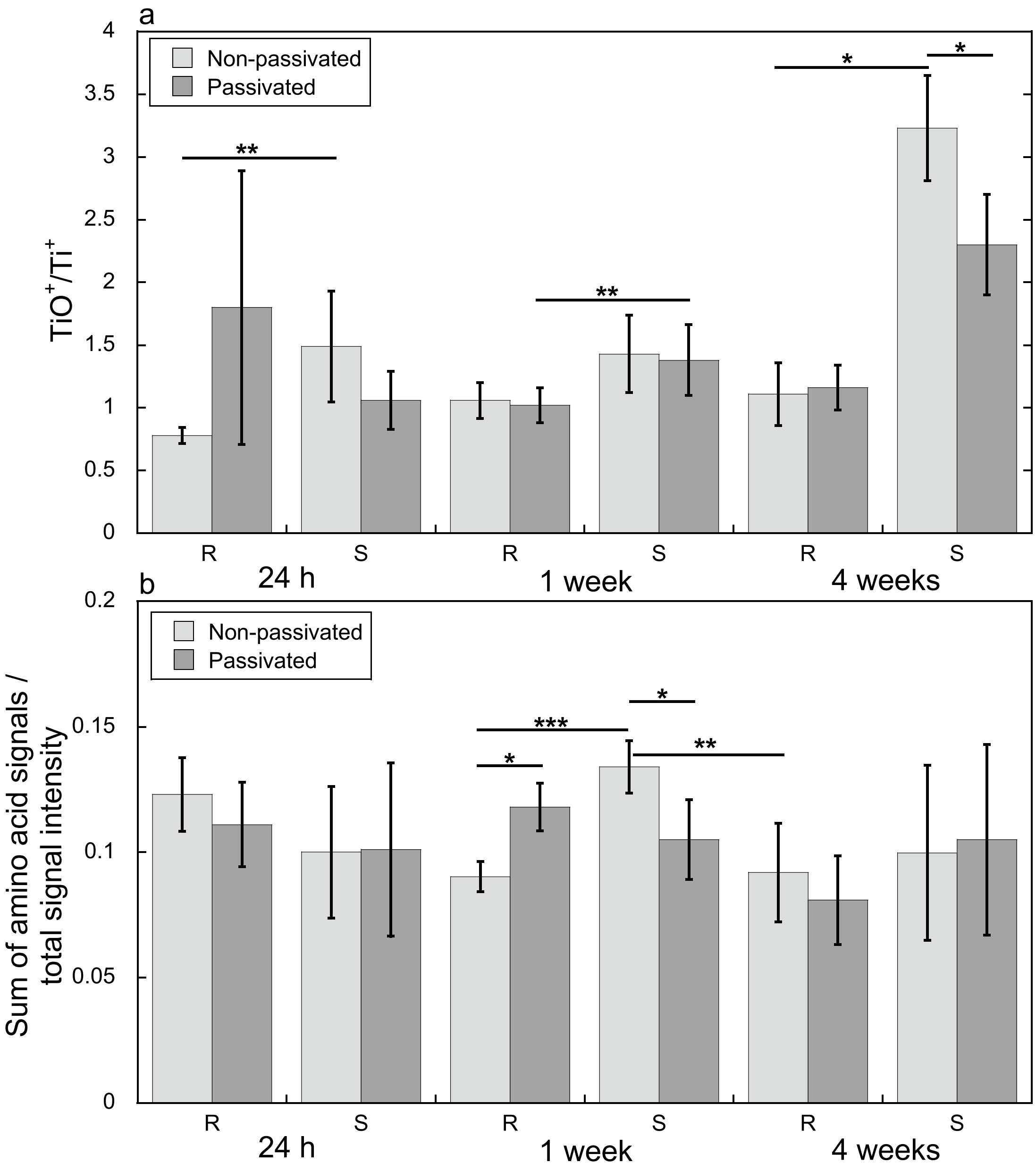

Fig. 8. Ratio of TiO^+ to Ti^+ (a) and sum of intensities of amino acid signature peaks normalized to total intensity (b) for the different surface conditions after 24 h, 1 week, and 4 weeks of exposure to BSA solution (5 g/L NaCl, 5 mM MES, 10 g/L BSA) at pH 7.4 and 25 °C. *$P < 0.05$; **$P < 0.01$; ***$P < 0.001$.

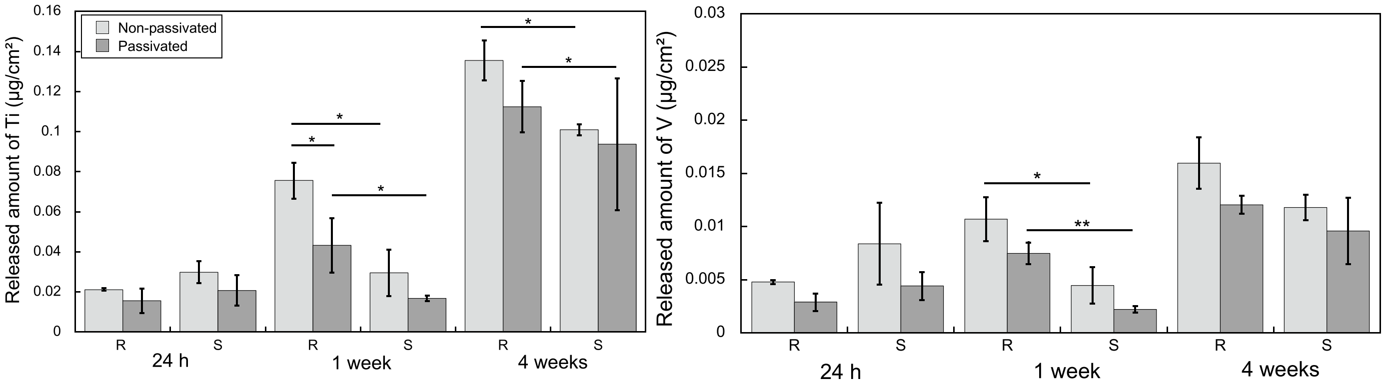

Fig. 9. Released amounts of Ti and V for different surface conditions after exposure to BSA solution (5 g/L NaCl, 5 mM MES, 10 g/L BSA) at pH 7.4 and 25 °C. *$P < 0.05$; **$P < 0.01$.

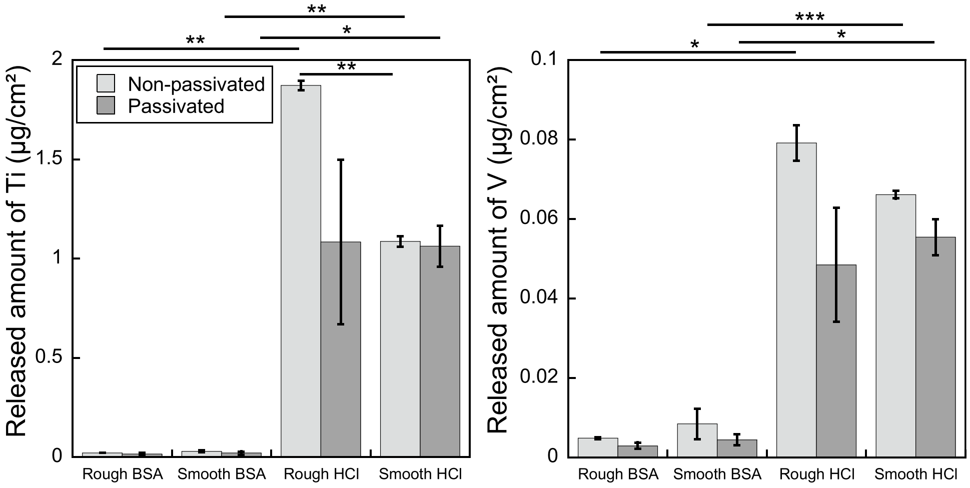

Fig. 10. Released amounts of Ti and V for different surface conditions after 25 °C 24 h exposure to BSA solution (5 g/L NaCl, 5 mM MES, 10 g/L BSA) at pH 7.4 and 0.027 M HCl (pH 1.5). **P* < 0.05; ***P* < 0.01; ****P* < 0.001.

1. Implanted ceramic beads from sandblasting remained on the surface after mirror-polishing and passivation.
2. Electrochemical measurements showed that passivation did not significantly change the corrosion resistance of the Ti6Al4V alloy in the BSA-containing solution (5 g/L NaCl, 5 mM MES, 10 g/L BSA, pH 7.4). In the BSA solution, all specimens remained passive.
3. The HCl solution resulted in significantly higher titanium and vanadium release than the neutral BSA solution after 24 h of immersion. However, no change in surface composition was observed after 24 h exposure to the HCl solution compared to unexposed surfaces.
4. Surface analysis revealed no significant impact of passivation. Rough specimens were shown to have a 10–20 % larger surface area. Rough surfaces had also a higher extent/compaction of protein adsorption, as identified by XPS and ToF-SIMS.
5. The mirror-polished smooth surfaces had a slightly thicker oxide with a higher ratio of aluminum oxide and fewer proteins adsorbed than the rough surfaces, even after 4 weeks of exposure to the BSA solution. These smooth surfaces also showed contamination from silicone and the ceramic sandblasting beads.
6. Passivation resulted in only a slightly lower titanium release from rough LPBF Ti6Al4V in both HCl (pH 1.5) and BSA-containing solution (pH 7.4).
7. This study shows a minor effect of passivation on corrosion resistance; however, passivation might be required for other reasons.

Funding

This work was supported by the center for Advanced Materials and Biomaterials Research, Western University [grant number 2021]; Natural Sciences and Engineering Research Council of Canada [grant numbers DGDND-2021–03997, RGPIN-2021–03997, RGPIN-2020–06856]; the Canada Research Chairs Program [grant number CRC-2019–00425]; the Wolfe-Western Fellowship [grant number 2020].

Data availability

Raw data is available on the platform Open Science Framework: https://osf.io/2djf6/?view_only=696c5db4925a462ab136c2378e44b898.

CRediT authorship contribution statement

Saman Nikpour: Investigation, Conceptualization, Methodology, Validation, Formal analysis, Writing – original draft, Visualization. **Jeffrey D. Henderson:** Investigation, Formal analysis, Writing – review & editing, Visualization. **Sina Matin:** Methodology, Writing – review & editing. **Heng-Yong Nie:** Methodology, Formal analysis, Supervision, Writing – review & editing. **Jonas Hedberg:** Methodology, Supervision, Writing – review & editing. **Vahid Dehnavi:** Methodology, Investigation, Formal analysis, Validation, Writing – review & editing. **Yara K. Hosein:** Conceptualization, Methodology, Resources, Writing – review & editing, Project administration, Funding acquisition. **David W. Holdsworth:** Resources, Writing – review & editing, Funding acquisition. **Mark Biesinger:** Conceptualization, Methodology, Supervision, Writing – review & editing, Funding acquisition. **Yolanda S. Hedberg:** Conceptualization, Methodology, Validation, Formal analysis, Resources, Writing – review & editing, Visualization, Supervision, Project administration, Funding acquisition.

Declaration of Competing Interest

The authors declare the following financial interests/personal relationships which may be considered as potential competing interests:

Yolanda Hedberg reports financial support was provided by center for Advanced Materials and Biomaterials Research. Yolanda Hedberg reports financial support was provided by Natural Sciences and Engineering Research Council of Canada. Yolanda Hedberg reports financial support was provided by Canada Research Chairs Program. Yolanda Hedberg reports financial support was provided by Western University. Yolanda Hedberg reports equipment, drugs, or supplies was provided by ADEISS.

Acknowledgement

We would like to acknowledge the assistance of Engineering Technician David Pacifico and Production Manager Tom Chmiel at Additive Design In Surgical Solutions, Inc., and the assistance of the analytical lab at Biotron, Western University.

Supplementary materials

Supplementary material associated with this article can be found, in the online version, at doi:10.1016/j.electacta.2023.143650.

References

[1] F. Trevisan, F. Calignano, A. Aversa, G. Marchese, M. Lombardi, S. Biamino, D. Ugues, D. Manfredi, Additive manufacturing of titanium alloys in the biomedical field: processes, properties and applications, J Appl Biomater Funct Mater 16 (2018) 57–67, https://doi.org/10.5301/jabfm.5000371.

[2] J.D. Avila, S. Bose, A. Bandyopadhyay, Additive manufacturing of titanium and titanium alloys for biomedical applications. Titanium in Medical and Dental Applications, Elsevier Inc., 2018, pp. 325–343, https://doi.org/10.1016/B978-0-12-812456-7.00015-9.

[3] S. Liu, Y.C. Shin, Additive manufacturing of Ti6Al4V alloy: a review, Mater. Des. 164 (2019), 107552, https://doi.org/10.1016/j.matdes.2018.107552.

[4] Q. Chen, G.A. Thouas, Metallic implant biomaterials, Mater. Sci. Eng. R: Rep. 87 (2015) 1–57, https://doi.org/10.1016/j.mser.2014.10.001.

[5] C.C. Willhite, N.A. Karyakina, R.A. Yokel, N. Yenugadhati, T.M. Wisniewski, I.M. F. Arnold, F. Momoli, D. Krewski, Systematic review of potential health risks posed by pharmaceutical, occupational and consumer exposures to metallic and nanoscale aluminum, aluminum oxides, aluminum hydroxide and its soluble salts, Crit. Rev. Toxicol. 44 (2014) 1–80, https://doi.org/10.3109/10408444.2014.934439.

[6] J.L. Domingo, Vanadium and diabetes. What about vanadium toxicity? Mol. Cell. Biochem. 203 (2000) 185–187, https://doi.org/10.1023/a:1007067011338.

[7] B. Kręcisz, M. Kieć-Świerczyńska, K. Bąkowicz-Mitura, Allergy to metals as a cause of orthopedic implant failure, Int. J. Occup. Med. Environ. Health 19 (2006) 178–180, https://doi.org/10.2478/v10001-006-0025-6.

[8] R.V. Badhe, O. Akinfosile, D. Bijukumar, M. Barba, M.T. Mathew, Systemic toxicity eliciting metal ion levels from metallic implants and orthopedic devices – A mini review, Toxicol. Lett. 350 (2021) 213–224, https://doi.org/10.1016/j.toxlet.2021.07.004.

[9] A. Decker, D. Daly, R.K. Scher, Role of titanium in the development of yellow nail syndrome, Skin Appendage Disord 1 (2015) 28–30, https://doi.org/10.1159/000375171.

[10] D. Krewski, R.A. Yokel, E. Nieboer, D. Borchelt, J. Cohen, J. Harry, S. Kacew, J. Lindsay, A.M. Mahfouz, V. Rondeau, Human health risk assessment for aluminium, aluminium oxide, and aluminium hydroxide, J. Toxicol. Environ. Health B Crit. Rev. 10 (2007) 1–269, https://doi.org/10.1080/10937400701597766.

[11] M.A. König, O.P. Gautschi, H.P. Simmen, L. Filgueira, D. Cadosch, Influence of vanadium 4+ and 5+ Ions on the differentiation and activation of human osteoclasts, Int J Biomater (2017) 2017, https://doi.org/10.1155/2017/9439036.

[12] M. Masmoudi, M. Assoul, M. Wery, R. Abdelhedi, F. El Halouani, G. Monteil, Wear behaviour of nitric acid passivated cp Ti and Ti6Al4V, J. Alloys Compd. 478 (2009) 726–730, https://doi.org/10.1016/j.jallcom.2008.11.138.

[13] P. Verdeguer, J. Gil, M. Punset, J.M. Manero, J. Nart, J. Vilarrasa, E. Ruperez, Citric acid in the passivation of titanium dental implants: corrosion resistance and bactericide behavior, Materials (Basel) (2022) 15, https://doi.org/10.3390/ma15020545.

[14] D.J. Fernandes, R.G. Marques, C.N. Elias, Influence of acid treatment on surface properties and in vivo performance of Ti6Al4V alloy for biomedical applications, J. Mater. Sci. Mater. Med. 28 (2017), https://doi.org/10.1007/s10856-017-5977-5.

[15] M. Masmoudi, M. Assoul, M. Wery, R. Abdelhedi, F. El Halouani, G. Monteil, Friction and wear behaviour of cp Ti and Ti6Al4V following nitric acid passivation, Appl. Surf. Sci. 253 (2006) 2237–2243, https://doi.org/10.1016/j.apsusc.2006.04.047.

[16] S. Ferraris, Y.S. Hedberg, J.J. Noël, S. Spriano, Interactions Between the Physiological Environment and Titanium-Based Implant Materials: from Understanding to Control. Nanoscale Engineering of Biomaterials: Properties and Applications, Springer Nature, Singapore, 2022, pp. 3–26, https://doi.org/10.1007/978-981-16-3667-7_1.

[17] T.M. Chiu, M. Mahmoudi, W. Dai, A. Elwany, H. Liang, H. Castaneda, Corrosion assessment of Ti-6Al-4V fabricated using laser powder-bed fusion additive manufacturing, Electrochim. Acta 279 (2018) 143–151, https://doi.org/10.1016/j.electacta.2018.04.189.

[18] E. Rezvani Ghomi, F. Khosravi, R.E. Neisiany, S. Singh, S. Ramakrishna, Future of additive manufacturing in healthcare, Curr Opin Biomed Eng 17 (2021), 100255, https://doi.org/10.1016/j.cobme.2020.100255.

[19] F.S.L. Bobbert, K. Lietaert, A.A. Eftekhari, B. Pouran, S.M. Ahmadi, H. Weinans, A. A. Zadpoor, Additively manufactured metallic porous biomaterials based on minimal surfaces: a unique combination of topological, mechanical, and mass transport properties, Acta Biomater. 53 (2017) 572–584, https://doi.org/10.1016/j.actbio.2017.02.024.

[20] G.R.M. Matos, Surface roughness of dental implant and osseointegration, J Maxillofac Oral Surg 20 (2021), https://doi.org/10.1007/s12663-020-01437-5.

[21] C. Cappellini, A. Malandruccolo, A. Abeni, A. Attanasio, A feasibility study of promoting osseointegration surface roughness by micro-milling of Ti-6Al-4V biomedical alloy, Int. J. Adv. Manuf. Technol. 126 (2023) 3053–3067, https://doi.org/10.1007/s00170-023-11318-z.

[22] Z. Wei, V. Romanovski, L. Filho, C. Persson, Y.S. Hedberg, Metal release from a biomedical CoCrMo alloy in mixed protein solutions under static and sliding conditions: effects of protein aggregation and metal precipitation, J Bio Tribocorros 8 (2022) 1–11, https://doi.org/10.1007/s40735-021-00617-1.

[23] G.W. Kubacki, J.L. Gilbert, The effect of the inflammatory species hypochlorous acid on the corrosion and surface damage of Ti-6Al-4V and CoCrMo alloys, J. Biomed. Mater. Res. A 106 (2018) 3185–3194, https://doi.org/10.1002/jbm.a.36513.

[24] J. Calvillo, M. Galicia, R. Malpica, E. Ordoñez, H.F. Pérez, Formation of Escherichia coli biofilms on the titanium alloy Ti6Al4V: analysis of the interface and assessment of corrosion, Corros. Eng. Sci. Technol. 56 (2021) 439–447, https://doi.org/10.1080/1478422X.2021.1901043.

[25] Y.S. Hedberg, Role of proteins in the degradation of relatively inert alloys in the human body, Npj Mater Degrad 2 (2018) 1–5, https://doi.org/10.1038/s41529-018-0049-y.

[26] J. Huang, A. Gonzalez Orive, J.T. Krüger, K.P. Hoyer, A. Keller, G. Grundmeier, Influence of proteins on the corrosion of a conventional and selective laser beam melted FeMn alloy in physiological electrolytes, Corros. Sci. 200 (2022), https://doi.org/10.1016/j.corsci.2022.110186.

[27] E. Liamas, O.R.T. Thomas, A.I. Muñoz, Z.J. Zhang, Tribocorrosion behaviour of pure titanium in bovine serum albumin solution: a multiscale study, J. Mech. Behav. Biomed. Mater. 102 (2020), https://doi.org/10.1016/j.jmbbm.2019.103511.

[28] S. Karimi, T. Nickchi, A. Alfantazi, Effects of bovine serum albumin on the corrosion behaviour of AISI 316L, Co-28Cr-6Mo, and Ti-6Al-4V alloys in phosphate buffered saline solutions, Corros. Sci. 53 (2011) 3262–3272, https://doi.org/10.1016/j.corsci.2011.06.009.

[29] J.L. Gilbert, Corrosion in the human body: metallic implants in the complex body environment, Corrosion 73 (2017) 1478–1495, https://doi.org/10.5006/2563.

[30] M.C. Biesinger, L.W.M. Lau, A.R. Gerson, R.S.C. Smart, Resolving surface chemical states in XPS analysis of first row transition metals, oxides and hydroxides: *sc*, Ti, V, Cu and Zn, Appl. Surf. Sci. 257 (2010) 887–898, https://doi.org/10.1016/j.apsusc.2010.07.086.

[31] D. Briggs, Edition. X-ray photoelectron spectroscopy (XPS), Handbook of Adhesion, second edition, 2005, pp. 621–622, https://doi.org/10.1002/0470014229.ch22.

[32] M.C. Biesinger, Accessing the robustness of adventitious carbon for charge referencing (correction) purposes in XPS analysis: insights from a multi-user facility data review, Appl. Surf. Sci. 597 (2022), 153681, https://doi.org/10.1016/j.apsusc.2022.153681.

[33] Y.S. Hedberg, M. Žnidaršič, G. Herting, I. Milošev, I. Odnevall Wallinder, Mechanistic insight on the combined effect of albumin and hydrogen peroxide on surface oxide composition and extent of metal release from Ti6Al4V, J. Biomed. Mater. Res. B Appl. Biomater. 107 (2019) 858–867, https://doi.org/10.1002/jbm.b.34182.

[34] L. Dragus, L. Benea, N. Simionescu, A. Ravoiu, V. Neaga, Effect of the inflammatory conditions and albumin presence on the corrosion behavior of grade 5 Titanium alloy in saliva biological solution, in: IOP Conf. Ser. Mater. Sci. Eng., 572, 2019, 012005, https://doi.org/10.1088/1757-899X/572/1/012005.

[35] L.Y. Chen, H.Y. Zhang, C. Zheng, H.Y. Yang, P. Qin, C. Zhao, S. Lu, S.X. Liang, L. Chai, L.C. Zhang, Corrosion behavior and characteristics of passive films of laser powder bed fusion produced Ti–6Al–4V in dynamic Hank's solution, Mater. Des. 208 (2021), 109907, https://doi.org/10.1016/j.matdes.2021.109907.

[36] M.E. Orazem, B. Tribollet, A tutorial on electrochemical impedance spectroscopy, ChemTexts 6 (2020) 1–9, https://doi.org/10.1007/s40828-020-0110-7.

[37] D. Fischer, K. yuan Cheng, M.Q. Neto, D. Hall, D. Bijukumar, A.A. Espinoza Orías, R. Pourzal, R.J. van Arkel, M.T. Mathew, Corrosion behavior of selective laser melting (SLM) Manufactured Ti6Al4V Alloy in Saline and BCS Solution, J Bio Tribocorros 8 (2022) 1–14, https://doi.org/10.1007/s40735-022-00657-1.

[38] B. Hirschorn, M.E. Orazem, B. Tribollet, V. Vivier, I. Frateur, M. Musiani, Determination of effective capacitance and film thickness from constant-phase-element parameters, Electrochim. Acta 55 (2010) 6218–6227, https://doi.org/10.1016/j.electacta.2009.10.065.

[39] R. Namus, W.M. Rainforth, The influence of cathodic potentials on the surface oxide layer status and tribocorrosion behaviour of Ti6Al4V and CoCrMo alloys in simulated body fluid, Biotribology 30 (2022), 100212, https://doi.org/10.1016/j.biotri.2022.100212.

[40] V. Gopal, G. Manivasagam, Wear – Corrosion synergistic effect on Ti–6Al–4V alloy in H2O2 and albumin environment, J. Alloys Compd. 830 (2020), 154539, https://doi.org/10.1016/j.jallcom.2020.154539.

[41] O. Klok, A.I. Munoz, S. Mischler, An overview of serum albumin interactions with biomedical alloys, Materials 13 (2020) 1–26, https://doi.org/10.3390/ma13214858 (Basel).

[42] N. Dai, L.C. Zhang, J. Zhang, X. Zhang, Q. Ni, Y. Chen, M. Wu, C. Yang, Distinction in corrosion resistance of selective laser melted Ti-6Al-4V alloy on different planes, Corros. Sci. 111 (2016) 703–710, https://doi.org/10.1016/j.corsci.2016.06.009.

[43] M. Atapour, A.L. Pilchak, M. Shamanian, M.H. Fathi, Corrosion behavior of Ti-8Al-1Mo-1V alloy compared to Ti-6Al-4V, Mater Des. 32 (2011) 1692–1696, https://doi.org/10.1016/j.matdes.2010.09.009.

[44] T. Peters, Serum Albumin, Adv. Protein Chem. 37 (1985) 161–245, https://doi.org/10.1016/S0065-3233(08)60065-0.

[45] K. Hirayama, S. Akashi, M. Furuya, K. ichi Fukuhara, Rapid confirmation and revision of the primary structure of bovine serum albumin by ESIMS and frit-FAB LC/MS, Biochem. Biophys. Res. Commun. 173 (1990) 639–646, https://doi.org/10.1016/S0006-291X(05)80083-X.

[46] Y. Hedberg, X. Wang, J. Hedberg, M. Lundin, E. Blomberg, I. Odnevall Wallinder, Surface-protein interactions on different stainless steel grades: effects of protein adsorption, surface changes and metal release, J. Mater. Sci. Mater. Med. 24 (2013) 1015–1033, https://doi.org/10.1007/s10856-013-4859-8.

[47] M. Lundin, Y. Hedberg, T. Jiang, G. Herting, X. Wang, E. Thormann, E. Blomberg, I. O. Wallinder, Adsorption and protein-induced metal release from chromium metal and stainless steel, J. Colloid Interface Sci. 366 (2012) 155–164, https://doi.org/10.1016/j.jcis.2011.09.068.

[48] M. Atapour, S. Sanaei, Z. Wei, M. Sheikholeslam, J.D. Henderson, U. Eduok, Y. K. Hosein, D.W. Holdsworth, Y.S. Hedberg, H.R. Ghorbani, In vitro corrosion and biocompatibility behavior of CoCrMo alloy manufactured by laser powder bed fusion parallel and perpendicular to the build direction, Electrochim. Acta 445 (2023), 142059, https://doi.org/10.1016/j.electacta.2023.142059.

[49] Y.S. Hedberg, M.S. Killian, E. Blomberg, S. Virtanen, P. Schmuki, I. Odnevall Wallinder, Interaction of bovine serum albumin and lysozyme with stainless steel studied by time-of-flight secondary ion mass spectrometry and X-ray photoelectron spectroscopy, Langmuir 28 (2012) 16306–16317, https://doi.org/10.1021/la3039279.

[50] J. Barberi, S. Spriano, Titanium and protein adsorption: an overview of mechanisms and effects of surface features, Materials (Basel) (2021) 14, https://doi.org/10.3390/ma14071590.

[51] M. Tagliazucchi, I. Szleifer, Stimuli-responsive polymers grafted to nanopores and other nano-curved surfaces: structure, chemical equilibrium and transport, Soft Matter 8 (2012) 7292–7305, https://doi.org/10.1039/c2sm25777g.

[52] I. Erukhimovich, M.O. de la Cruz, Phase equilibria and charge fractionation in polydisperse polyelectrolyte solutions, J. Polym. Sci. B Polym. Phys. 44 (2004) 2638–2662, https://doi.org/10.1002/polb.

[53] M. Lundqvist, I. Sethson, B.H. Jonsson, Protein adsorption onto silica nanoparticles: conformational changes depend on the particles' curvature and the protein stability, Langmuir. 20 (2004) 10639–10647, https://doi.org/10.1021/la0484725.

[54] F. Yu, O. Addison, A.J. Davenport, A synergistic effect of albumin and H2O2 accelerates corrosion of Ti6Al4V, Acta Biomater. 26 (2015) 355–365.

[55] B.W. Callen, B.F. Lowenberg, S. Lugowski, R.N.S. Sodhi, J.E. Davies, Nitric acid assivation of Ti6A14V reduces thickness of surface oxi e, J. Biomed. Mater. Res. B Appl. Biomater. 29 (1995) 279–290, https://doi.org/10.1002/jbm.820290302.

[56] S. Karimi, A.M. Alfantazi, Ion release and surface oxide composition of AISI 316L, Co-28Cr-6Mo, and Ti-6Al-4V alloys immersed in human serum albumin solutions, Mater. Sci. Eng. C 40 (2014) 435–444, https://doi.org/10.1016/j.msec.2014.04.007.

[57] Y.S. Hedberg, F. Gamna, G. Padoan, S. Ferraris, M. Cazzola, G. Herting, M. Atapour, S. Spriano, I. Odnevall Wallinder, Surface modified Ti6Al4V for enhanced bone bonding ability – Effects of silver and corrosivity at simulated physiological conditions from a corrosion and metal release perspective, Corros. Sci. 168 (2020), 108566, https://doi.org/10.1016/j.corsci.2020.108566.

[58] Y. Okazaki, E. Gotoh, Comparison of metal release from various metallic biomaterials in vitro, Biomaterials 26 (2005) 11–21, https://doi.org/10.1016/j.biomaterials.2004.02.005.

[59] A.V. Davey, The effect of manufacturing techniques on custom-made titanium cranioplasty plates : a pilot study, J. Craniomaxillofac. Surg. 45 (2017) 2017–2027, https://doi.org/10.1016/j.jcms.2017.09.020.

[60] M.J. Cardona, C. Turner, C. Ross, E. Baird, R.A. Black, An improved process for the fabrication and surface treatment of custom-made titanium cranioplasty implants informed by surface analysis, J. Biomater. Appl. 35 (2021) 602–614, https://doi.org/10.1177/0885328220957899.

[61] W. Xu, B. Zhang, O. Addison, X. Wang, Mechanically-assisted crevice corrosion and its effect on materials degradation, Corros. Prot. Offshore Commun. Symp. Int. 11 (2023) 23–32, https://doi.org/10.1016/j.corcom.2023.01.002.

[62] V. Barranco, M.L. Escudero, M.C. García-Alonso, 3D, chemical and electrochemical characterization of blasted TI6Al4V surfaces: its influence on the corrosion behaviour, Electrochim. Acta 52 (2007) 4374–4384, https://doi.org/10.1016/j.electacta.2006.12.031.

[63] A.A. Ragab, R. Van De Motter, S.A. Lavish, V.M. Goldberg, J.T. Ninomiya, C. R. Carlin, E.M. Greenfield, Measurement and removal of adherent endotoxin from titanium particles and implant surfaces, J. Orthop. Res. 17 (1999) 803–809, https://doi.org/10.1002/jor.1100170603.